Vol. 86: 169–184, 2021
https://doi.org/10.3354/ame01964

AQUATIC MICROBIAL ECOLOGY
Aquat Microb Ecol

Published online May 6

Swimming behavior of cryptophyte prey affects prey preference of the ambush-feeding ciliate *Mesodinium rubrum*

Houshuo Jiang[1,*], Matthew D. Johnson[2]

[1]Applied Ocean Physics and Engineering Department, Woods Hole Oceanographic Institution, Woods Hole, MA 02543, USA
[2]Biology Department, Woods Hole Oceanographic Institution, Woods Hole, MA 02543, USA

ABSTRACT: The mixotrophic ciliate *Mesodinium rubrum* is an ambush feeder relying on cryptophyte prey motility for prey encounter and perception; therefore, cryptophyte species-specific swimming behaviors affect *M. rubrum*'s prey preference. Here, a high-speed microscale imaging system was used to quantify the swimming behaviors of 3 cryptophyte species (*Teleaulax amphioxeia*, *Storeatula major*, and *Guillardia theta*) and to conduct quantitative microvideography of *M. rubrum*–*T. amphioxeia* predator–prey interaction. *T. amphioxeia*, a preferred prey of *M. rubrum*, swam at path-averaged speeds of 155 ± 73 µm s^{-1} along rather straight paths. In contrast, *S. major* regularly tumbled slowly downward or upward at 64 ± 16 µm s^{-1}, while *G. theta* moved slowly in looped/curved trajectories at 57 ± 15 µm s^{-1}; neither supports *M. rubrum* growth. Only while motionlessly sinking passively did *M. rubrum* detect and initiate an attack on swimming *T. amphioxeia* at reaction distances of 8.2 ± 8.2 µm. It seemed that *M. rubrum* needed to use oral tentacles to initially poke *T. amphioxeia*'s ventral posterior part and subsequently poke the prey multiple times in a short duration to compromise the prey's escape ability, presumably by discharging extrusomes into the prey. *T. amphioxeia* also responded to nearby predators by switching to tumbling similar to *S. major* in normal swimming, suggesting an effective anti-predator defense behavior that prevents *M. rubrum* from accurately poking the prey's ventral posterior part. *T. amphioxeia* swimming at significantly higher speeds leads to sufficiently high prey encounters and hydrodynamic signals for *M. rubrum*, thereby partially explaining *M. rubrum*'s ability to select *T. amphioxeia* prey.

KEY WORDS: *Mesodinium rubrum* · Cryptophyte · Predator–prey interaction · Ambush feeding · Swimming behavior · Prey preference · High-speed microscale imaging system · HSMIS

1. INTRODUCTION

Predator–prey interactions in marine planktonic protists, just as any predator–prey interactions, are evolutionary arms races. Over evolutionary time, predators are selected to encounter, detect, attack, and capture prey more efficiently and effectively, while prey are chosen to become more adept at detecting and avoiding predators (Lima & Dill 1990, Ferrari et al. 2010). Consequently, protistan predator–prey interactions are strongly mediated by behavioral, morphological, and physiological traits of both predator and prey during their lifetime. To get a higher chance of a favorable outcome, both parties thrive to gain an information advantage by competing to remotely detect the other first. Such remote detection in protists is realized via chemoreception (Spero 1985, Buskey 1997, Harvey et al. 2013, Jiang et al. 2018) or mechanoreception (Jakobsen 2002, Jakobsen et al. 2006, Jiang et al. 2018). Since they are mostly microscopic and slow moving relative to the macroscopic world, the generation and transmission of hydrodynamic and chemical signals of protists are governed by low Reynolds number fluid dynamics together

*Corresponding author: hsjiang@whoi.edu

with small-scale diffusion (e.g. Jiang 2011, Kiørboe et al. 2014, Jiang & Johnson 2017).

The mixotrophic ciliate *Mesodinium rubrum* ingests cryptophyte prey of the *Teleaulax/Plagioselmis/Geminigera* (TPG) clade to sequester a nucleus, plastids, and other cell organelles for sustained photosynthesis and growth (Gustafson et al. 2000, Johnson et al. 2007, Park et al. 2007, Smith & Hansen 2007, Myung et al. 2011, Hansen et al. 2012, Peltomaa & Johnson 2017). When feeding on its preferred prey (*Teleaulax* spp.), temperate *M. rubrum* needs only ~1 cell d^{-1} to achieve its maximum growth rate (Smith & Hansen 2007). This ingestion rate amounts to only 1 to 2% of the required carbon per day, illustrating that *M. rubrum* is almost entirely phototrophic (Johnson & Stoecker 2005). Nevertheless, the availability of TPG cryptophyte prey is necessary for *M. rubrum* to achieve maximum growth rates under laboratory conditions (Park et al. 2007, Myung et al. 2011) and to form high-productivity blooms in the field (Herfort et al. 2011, Peterson et al. 2013, Johnson et al. 2016). Thus, the TPG prey preference is a crucial feature of the predator–prey interaction between *M. rubrum* and its cryptophyte prey; however, a mechanistic understanding of such a preference is still lacking.

Despite the lack of direct observational evidence, *M. rubrum* is (likely) an active ambush feeder, as defined by Kiørboe (2011), that passively encounters/perceives a motile prey and then actively attacks it for capture, similar to what was shown previously for the heterotrophic ciliate *M. pulex* (Jakobsen et al. 2006). The ingestion of cryptophyte prey by *M. rubrum* was documented previously by using video imaging microscopy (Yih et al. 2004); however, the individual-level behavior and kinematics of the predator–prey interaction remain undocumented, including encounter and perception between the predator and prey, prey capture by the predator, and predator avoidance by the prey.

Cryptophyte algae have 2 slightly unequal flagella (Hibberd et al. 1971), and the longer flagellum pulls the cell to swim (Hoef-Emden & Archibald 2017). They also possess ejectosomes that, when explosively discharged, propel the cell away from perceived danger by abruptly changing swimming direction and moving in a jerky fashion (Hoef-Emden & Archibald 2017). Despite current knowledge, the swimming kinematics and species-specific swimming behaviors of cryptophytes have not yet been documented.

Ambush feeders depend on prey motility for encountering and perceiving prey (Svensen & Kiørboe 2000, Jakobsen et al. 2006) and may use prey species-specific hydrodynamic signals to distinguish among prey species (Jiang & Paffenhöfer 2008). Along this line of research, the present study used a high-speed microscale imaging system (HSMIS) to observe and quantify swimming behaviors and kinematics of 3 cryptophyte species; namely, *Teleaulax amphioxeia*, *Storeatula major*, and *Guillardia theta*. As mentioned above, *T. amphioxeia* is a preferred prey of *M. rubrum*, while neither *S. major* (Peltomaa & Johnson 2017) nor *G. theta* (Hansen et al. 2012) supports the growth of *M. rubrum*, and neither belongs to the TPG clade. The HSMIS was also used to conduct quantitative microvideography of the predator–prey interaction between *M. rubrum* and *T. amphioxeia*. The present study aimed to shed light on a mechanistic understanding of the TPG prey preference of *M. rubrum*.

2. MATERIALS AND METHODS

2.1. Culture maintenance

Three cryptophyte species were used in this study: *Teleaulax amphioxeia* (GCEP01), isolated from Eel Pond, Falmouth, MA, by Mengmeng Tong; *Storeatula major* (strain SM or g), isolated from the Choptank River, Cambridge, MD, by Alan Lewitus; and *Guillardia theta* (CCMP 2712), obtained from the National Center for Marine Algae and Microbiota, Bigelow Laboratory, East Boothbay, ME, USA. The *T. amphioxeia* cultures were maintained in 250 ml flasks in 15 and 32 PSU f/2 medium at 15°C with an irradiance of 54 µmol photons m^{-2} s^{-1} on a 14 h light:10 h dark photoperiod, while the *S. major* and *G. theta* cultures were maintained similarly but only in 32 PSU f/2 medium. The diploid *T. amphioxeia*, not its haploid form (*Plagioselmis prolonga*), was used in this study (see Altenburger et al. 2020).

Cultures of *Mesodinium rubrum* (strain MR2A1), previously isolated from the mouth of the James River in Chesapeake Bay, were acclimated to and maintained in the same conditions as their cryptophyte prey. For routine maintenance, cultures of *T. amphioxeia* were fed to *M. rubrum* once per week. All experiments using *T. amphioxeia* were conducted at 15 PSU, while experiments with *S. major* and *G. theta* were conducted at 32 PSU. The reason for using different salinities was because, at the time, *M. rubrum* was growing better on *T. amphioxeia* at 15 PSU for unclear reasons. The stock cultures of *M. rubrum* were allowed to graze down their prey prior to experiments, when fresh prey were then added (see Section 2.3).

2.2. High-speed microvideography

Quantitative microvideography was conducted by using the HSMIS to observe cryptophyte species-specific swimming behaviors and the predator–prey interaction between *M. rubrum* and *T. amphioxeia*. A similar approach has been previously used to observe protists (Jiang & Johnson 2017, Jiang et al. 2018) and copepod nauplii (Jiang & Paffenhöfer 2020) but with different optical specifications. The optical setup of this study consisted of a 200 mm focal length objective lens plus an infinity-corrected, long working distance microscope objective (50×/0.45, 17.0 mm working distance). The optical setup was mounted horizontally to a Photron FASTCAM SA3 120K monochrome video camera, resulting in a vertically oriented field of view area of ~368 × 368 µm. The camera took 1024 × 1024 pixel resolution images at a frame rate of 2000 frames s^{-1}. Backlit illumination was used, where a 1 W white LED light source was collimated to shine light through a small transparent water vessel towards the camera. The vessel, placed in front of the microscope objective, was either a glass cuvette (12.5 × 12.5 × 45 mm) or a 25 ml tissue culture flask (26 × 44 × 82 mm). The center of the cuvette (flask) was focused; thus, the field of view was more than 5 (10) mm away from the walls of the cuvette (flask). Observations were conducted in a temperature-controlled room of ~19°C.

2.3. Behavioral observations

Swimming behaviors of the 3 cryptophyte species were observed, respectively, on 3 individual days. For each species, 2 glass cuvettes, each holding ~2 ml cryptophyte culture, were prepared and then acclimated in the temperature-controlled room for ~2 h. After acclimation, the cells in each cuvette were observed for their swimming behavior by using the HSMIS, and the observation on each cuvette lasted ~2 h. The cell concentrations were 134 300 cells ml^{-1} for *T. amphioxeia*, 120 840 cells ml^{-1} for *S. major*, and 98 670 cells ml^{-1} for *G. theta*.

The predator–prey interaction between *M. rubrum* and *T. amphioxeia* was also observed on 3 individual days. On each day, two 25 ml flasks, each holding ~15 ml *M. rubrum* culture (14 600–18 530 cells ml^{-1}), and 1 tube of ~15 ml *T. amphioxeia* culture (134 300–167 300 cells ml^{-1}) were prepared and then acclimated in the temperature-controlled room for ~2 h. After acclimation, the jumping behavior of *M. rubrum* in one flask was observed first for ~40 min without adding the prey *T. amphioxeia*. Then, ~5 ml prey solution was introduced to the flask, resulting in 33 575 to 41 825 and 10 950 to 13 898 cells ml^{-1} of *T. amphioxeia* and *M. rubrum*, respectively, and a prey:predator ratio of ~3. Upon mixing, the flask was immediately placed on the stage of the HSMIS, and the predator–prey interaction inside the flask was observed for 20 to 40 min. The same observation procedure was repeated for the other flask. During each above-mentioned observation, many events were recorded as high-speed digital videos where cells swam and/or interacted within the HSMIS plane of focus. Similar observations were also conducted by mixing *M. rubrum* with *S. major* and *G. theta*, respectively, trying to finding out possible interactions; however, no visually discernible interactions were identified, and therefore no data could be reported. In these observations, *M. rubrum* cultures maintained in 32 PSU f/2 medium were used.

2.4. Video processing and data analysis

ImageJ software was used to process the high-speed digital videos and measure cell lengths (L_{Ta}, L_{Sm}, and L_{Gt}) and widths (W_{Ta}, W_{Sm}, and W_{Gt}) for the 3 cryptophyte species and cell length (L_{Mr}) and width (W_{Mr}) for *M. rubrum*. Behavioral and kinematic parameters of both cell movements and predator–prey interactions were also measured and calculated. For events of cryptophyte swimming, jumping, sinking, or tumbling, the parameters included, whenever applicable, event duration, path-averaged speed (U_{ave}), net to gross displacement ratio (NGDR; calculated using a time step of 0.5 ms), jump duration (t_{jump}), maximum jump speed (U_{max}), jump distance (d_{jump}), averaged sinking speed (U_{sink}), and tumble period (T_{tumble}). For events of *M. rubrum* jumping or sinking, the parameters included jump duration (t_{jump}), maximum jump speed (U_{max}), jump distance (d_{jump}), and averaged sinking speed (U_{sink}).

For events of the predator–prey interaction between *M. rubrum* and *T. amphioxeia*, the parameters included the reaction distance of an *M. rubrum* predator to a perceived *T. amphioxeia* prey (R_{Mr}), the reaction distance of a *T. amphioxeia* prey to an *M. rubrum* predator (R_{Ta}), and the speed of the *T. amphioxeia* prey right before the reaction happened (U_{Ta}). Videos of predator–prey interaction events were inspected to determine R_{Mr} as the nearest surface-to-surface distance between the predator and the prey when the predator reacted to the prey and R_{Ta} as the nearest surface-to-surface distance between the prey

and the predator when the prey started to escape by jumping away from the predator.

The graphing and data analysis software KaleidaGraph version 4.5.2 (Synergy Software) was used to run statistics and conduct Student's *t*-test (unpaired data with unequal variance) when determining if the means of 2 datasets were significantly different from each other, with a significance level of $p < 0.05$.

3. RESULTS

3.1. Swimming behaviors of the 3 cryptophyte species

The cryptophytes *Teleaulax amphioxeia*, *Storeatula major*, and *Guillardia theta* displayed distinct swimming behaviors. Cells of *T. amphioxeia* swam along rather straight and long paths (Fig. 1A; Event A of Video Group S1 at www.int-res.com/articles/suppl/a086p169_supp/) but also sporadically jumped at elevated speeds (Fig. 1B; Event B of Video Group S1). Cells of *S. major* regularly tumbled slowly downward or upward (Fig. 1C,D; Events C and D of Video Group S1). Cells of *G. theta* moved slowly in looped or curved trajectories (Fig. 1E,F; Events E and F of Video Group S1).

The 3 cryptophyte species also differed significantly in swimming kinematics. When alone, *T. amphioxeia* swam at path-averaged speeds of 155 ± 73 µm s^{-1} (11.2 ± 5.2 L_{Ta} s^{-1}) with NGDRs of 0.790 ± 0.141 (Table 1A), sporadically accelerated/jumped spontaneously at maximum speeds of 614 ± 70 µm s^{-1} (40.4 ± 8.2 L_{Ta} s^{-1}) and distances of 75 ± 45 µm (4.7 ± 2.7 L_{Ta}) (Table 1B), or occasionally sank at speeds of 101 ± 38 µm s^{-1} (7.1 ± 3.7 L_{Ta} s^{-1}) (Table 1C). In the presence of *Mesodinium rubrum*, *T. amphioxeia* swam at path-averaged speeds of 229 ± 111 µm s^{-1} (17.2 ± 8.7 L_{Ta} s^{-1}) (Table 1D), significantly faster than in the absence of the predator (Fig. 2A,B; Student's *t*-test, $p = 0.012$); the trajectories were more zigzagging with smaller NGDRs of 0.615 ± 0.310 (Table 1D) than in the absence of the predator (Fig. 2C; Student's *t*-test, $p = 0.025$). Escape jumping of *T. amphioxeia* attained maximum speeds of 616 ± 54 µm s^{-1} (48.1 ± 6.1 L_{Ta} s^{-1}) (Table 1E), similar to spontaneous accelerating/jumping; escape jump distances were 87 ± 40 µm (6.9 ± 3.6 L_{Ta}) (Table 1E), longer than spontaneous accelerating/jumping (albeit not statistically significant).

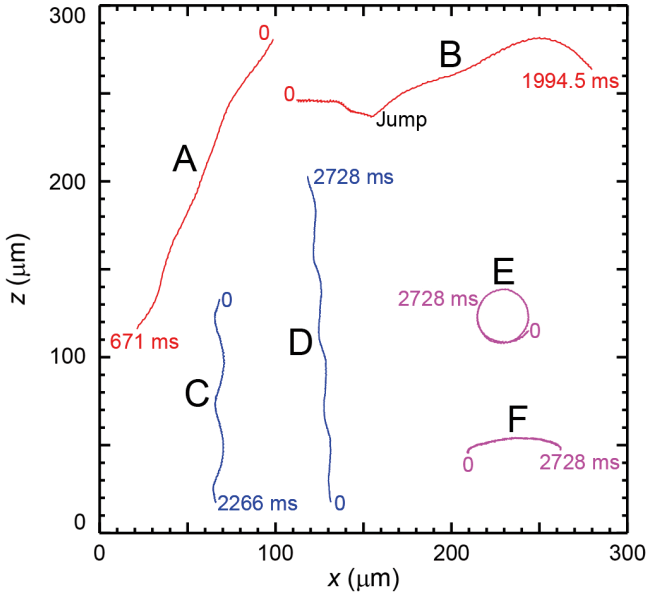

Fig. 1. Examples of cryptophyte swimming paths for *Teleaulax amphioxeia* (A,B; Events A and B of Video Group S1), *Storeatula major* (C,D; Events C and D of Video Group S1), and *Guillardia theta* (E,F; Events E and F of Video Group S1)

S. major swam by tumbling at path-averaged speeds of 64 ± 16 µm s^{-1} (5.2 ± 1.4 L_{Sm} s^{-1}) (Table 2A), significantly slower than *T. amphioxeia* in the absence of *M. rubrum* (Fig. 2A,B; Student's *t*-test, $p < 0.0001$); the tumbling trajectories were more zigzagging with smaller NGDRs of 0.518 ± 0.232 (Table 2A) than *T. amphioxeia* (Fig. 2C; Student's *t*-test, $p < 0.0001$); the tumbling periods were 782 ± 126 ms (Table 2A). The tumbling direction of *S. major* was dominantly vertical, either upward or downward, in sharp contrast to the more evenly distributed swimming directions of *T. amphioxeia* and *G. theta* (Fig. 3C vs. Fig. 3A,B,D). Although much less frequently, *S. major* also swam in non-tumbling ways (e.g. spiraling, rotating, or shaking) at speeds, NGDRs, and periods similar to tumbling (Table 2B). Occasionally, *S. major* sank at speeds of 33 ± 11 µm s^{-1} (2.5 ± 0.9 L_{Sm} s^{-1}) (Table 2C), significantly slower than sinking *T. amphioxeia* (Student's *t*-test, $p = 0.006$).

G. theta swam at path-averaged speeds of 57 ± 15 µm s^{-1} (6.2 ± 1.7 L_{Gt} s^{-1}) (Table 3), significantly slower than *T. amphioxeia* in the absence of *M. rubrum* (Fig. 2A,B; Student's *t*-test, $p < 0.0001$); the swimming trajectories were looped or curved with much smaller NGDRs of 0.263 ± 0.159 (Table 3) than *T. amphioxeia* (Fig. 2C; Student's *t*-test, $p < 0.0001$).

3.2. Motile behavior of *Mesodinium rubrum*

M. rubrum frequently jumped spontaneously at maximum jump speeds of 5.9 ± 1.4 mm s^{-1} (251.4 ± 53.7 L_{Mr} s^{-1}), covering jump distances of 97 ± 32 µm

Table 1. Analysis summary of the motile behavior of the marine cryptophyte *Teleaulax amphioxeia* (Ta)

A. Swimming

	Cell length (L_{Ta}) (µm)	Body width (W_{Ta}) (µm)	Event duration (ms)	Path-averaged speed (U_{ave}) (µm s^{-1})	(L_{Ta} s^{-1})	Net to gross displacement ratio (NGDR)
Mean ± SD	13.8 ± 1.9	7.5 ± 1.0	1281.8 ± 671.2	155 ± 73	11.2 ± 5.2	0.790 ± 0.141
Range	8.8–17.6	5.3–10.4	222.5–2728.0	52–297	3.8–20.9	0.378–0.955
n	33	33	38	38	38	38

B. Spontaneous accelerating/jumping

	Cell length (L_{Ta}) (µm)	Cell width (W_{Ta}) (µm)	Jump duration (t_{jump}) (ms)	Maximum jump speed (U_{max}) (µm s^{-1})	(L_{Ta} s^{-1})	Jump distance (d_{jump}) (µm)	(L_{Ta})
Mean ± SD	15.5 ± 1.7	7.8 ± 0.5	324 ± 201	614 ± 70	40.4 ± 8.2	75 ± 45	4.7 ± 2.7
Range	13.1–17.6	6.9–8.3	110–620	527–689	30.0–52.6	25–128	1.9–7.9
n	7	7	7	7	7	7	7

C. Sinking

	Cell length (L_{Ta}) (µm)	Body width (W_{Ta}) (µm)	Event duration (ms)	Averaged sinking speed (U_{sink}) (µm s^{-1})	(L_{Ta} s^{-1})
Mean ± SD	15.1 ± 3.0	7.7 ± 1.6	2039.6 ± 328.2	101 ± 38	7.1 ± 3.7
Range	10.2–17.9	5.3–9.1	1377.0–2255.0	65–150	3.8–13.0
n	6	6	6	6	6

D. Swimming in the presence of the ciliate predator *Mesodinium rubrum*

	Cell length (L_{Ta}) (µm)	Body width (W_{Ta}) (µm)	Event duration (ms)	Path-averaged speed (U_{ave}) (µm s^{-1})	(L_{Ta} s^{-1})	Net to gross displacement ratio (NGDR)
Mean ± SD	13.5 ± 1.9	6.6 ± 0.8	1186.6 ± 724.9	229 ± 111	17.2 ± 8.7	0.615 ± 0.310
Range	10.7–18.6	5.3–8.0	141.5–2728.0	49–379	4.2–34.4	0.0845–0.958
n	17	17	20	20	20	20

E. Escape jumping

	Cell length (L_{Ta}) (µm)	Cell width (W_{Ta}) (µm)	Jump duration (t_{jump}) (ms)	Maximum jump speed (U_{max}) (µm s^{-1})	(L_{Ta} s^{-1})	Jump distance (d_{jump}) (µm)	(L_{Ta})
Mean ± SD	12.9 ± 1.1	6.2 ± 0.9	299 ± 160	616 ± 54	48.1 ± 6.1	87 ± 40	6.9 ± 3.6
Range	12.0–14.5	5.4–7.8	140–536	562–701	41.7–56.1	39–148	2.7–12.4
n	5	5	5	5	5	5	5

(4.2 ± 1.4 L_{Mr}) within jump durations of 51 ± 9 ms (Table 4A). Between jumps, *M. rubrum* sank at speeds of 66 ± 22 µm s^{-1} (2.7 ± 0.8 L_{Mr} s^{-1}) (Table 4B).

In the presence of the cryptophyte prey *T. amphioxeia*, *M. rubrum* cells that had successfully captured a prey also jumped spontaneously while towing the captured prey (Table 4C). The maximum jump speeds were 4.9 ± 1.3 mm s^{-1} (199.4 ± 43.4 L_{Mr} s^{-1}), slower than in the absence of prey (Student's *t*-test, p = 0.05); the jump distances were 79 ± 28 µm (3.2 ± 0.9 L_{Mr}), shorter than in the absence of prey (Student's *t*-test, p = 0.09); the jump durations were 42 ± 5 ms, briefer than in the absence of prey (Student's

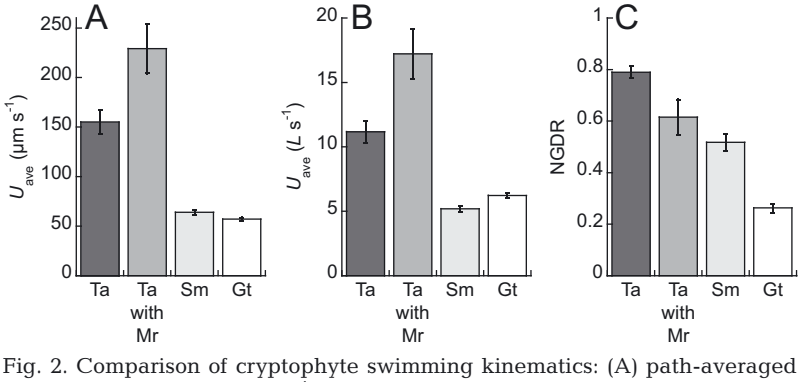

Fig. 2. Comparison of cryptophyte swimming kinematics: (A) path-averaged swimming speed (U_{ave}, µm s^{-1}), (B) path-averaged swimming speed (U_{ave}, cell length [L] s^{-1}), and (C) net to gross displacement ratio (NGDR) for different species and situations, i.e. *Teleaulax amphioxeia* (Ta), *T. amphioxeia* in the presence of the ciliate predator *Mesodinium rubrum* (Ta with Mr), St*oreatula major* (Sm), and *Guillardia theta* (Gt). Error bars represent SEs

Table 2. Analysis summary of the motile behavior of the marine cryptophyte *Storeatula major* (Sm)

A. Swimming by tumbling

	Cell length (L_{Sm}) (µm)	Body width (W_{Sm}) (µm)	Event duration (ms)	Path-averaged speed (U_{ave}) (µm s^{-1})	(L_{Sm} s^{-1})	Net to gross displacement ratio (NGDR)	Tumble period (T_{tumble}) (ms)
Mean ± SD	12.4 ± 1.3	7.4 ± 1.0	2552.6 ± 288.9	64 ± 16	5.2 ± 1.4	0.518 ± 0.232	782 ± 126
Range	10.0–15.3	5.5–9.4	1771.0–2728.0	39–98	2.7–8.5	0.034–0.904	510–1090
n	47	47	47	47	47	47	47

B. Swimming in non-tumbling ways (e.g. spiraling, rotating, or shaking)

	Cell length (L_{Sm}) (µm)	Body width (W_{Sm}) (µm)	Event duration (ms)	Path-averaged speed (U_{ave}) (µm s^{-1})	(L_{Sm} s^{-1})	Net to gross displacement ratio (NGDR)	Movement period (T) (ms)
Mean ± SD	12.1 ± 1.6	7.2 ± 1.0	2710.0 ± 59.7	60 ± 22	5.0 ± 1.6	0.519 ± 0.223	924 ± 246
Range	9.5–15.7	5.6–8.7	2530.0–2728.0	34–96	2.8–7.6	0.085–0.781	610–1365
n	11	11	11	11	11	11	11

C. Sinking

	Cell length (L_{Sm}) (µm)	Body width (W_{Sm}) (µm)	Event duration (ms)	Averaged sinking speed (U_{sink}) (µm s^{-1})	(L_{Sm} s^{-1})
Mean ± SD	12.5 ± 0.3	7.4 ± 0.4	2451.4 ± 666.3	33 ± 11	2.5 ± 0.9
Range	12.1–12.9	6.7–7.8	946.0–2728.0	22–49	1.8–3.8
n	4	7	7	7	4

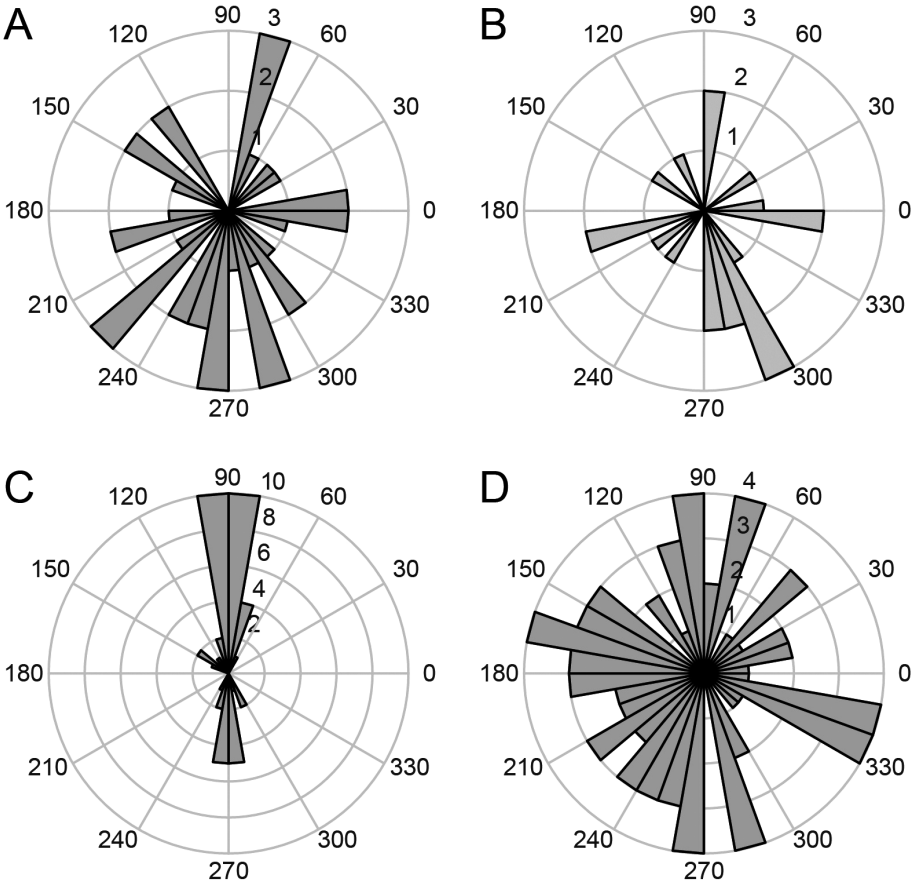

Fig. 3. Rose plots of the net swimming direction pointing from start to end of a swimming path for (A) *Teleaulax amphioxeia*, (B) *T. amphioxeia* in the presence of *Mesodinium rubrum*, (C) *Storeatula major*, and (D) *Guillardia theta*

Table 3. Analysis summary of the motile swimming behavior of the marine cryptophyte *Guillardia theta* (Gt)

	Cell length (L_{Gt}) (µm)	Body width (W_{Gt}) (µm)	Event duration (ms)	Path-averaged speed (U_{ave}) (µm s^{-1})	(L_{Gt} s^{-1})	Net to gross displacement ratio (NGDR)
Mean ± SD	9.2 ± 1.2	6.0 ± 0.8	2616.8 ± 302.6	57 ± 15	6.2 ± 1.7	0.263 ± 0.159
Range	6.9–12.4	4.6–8.6	1155.0–2728.0	31–88	3.3–10.0	0.040–0.811
n	81	81	81	81	81	81

t-test, p = 0.0002). Between jumps, those *M. rubrum* cells that were towing a captured prey also sank at speeds of 95 ± 31 µm s^{-1} (4.2 ± 1.5 L_{Mr} s^{-1}) (Table 4D).

3.3. Predator–prey interaction between *Mesodinium rubrum* and *Teleaulax amphioxeia*

HSMIS observations showed that *M. rubrum* was an ambush predator. Only while motionlessly sinking passively did an *M. rubrum* cell detect and initiate an attack on a nearby swimming or approaching *T. amphioxeia* cell (Figs. 4 & 5; Events A and B of Video Group 2 at www.int-res.com/articles/suppl/a086p169_supp/). Reaction distances of *M. rubrum* to *T. amphioxeia* were 8.2 ± 8.2 µm (with a range of 0–19 µm and n = 6) (Table 5A). Swimming speeds of *T. amphioxeia* right before *M. rubrum* started to react were 189 ± 70 µm s^{-1} (Table 5A).

HSMIS observations revealed in great detail that *M. rubrum* used oral tentacles to poke a detected *T. amphioxeia* cell. In a successful ambush-feeding event (Event A of Video Group 2), the *M. rubrum* predator pulled back and used its oral tentacles to poke the ventral posterior part of the *T. amphioxeia* prey as soon as the prey arrived sideways in front of

Table 4. Analysis summary of the motile behavior of the ciliate *Mesodinium rubrum* (Mr)

A. Spontaneous jumping, including jumping by tumbling

	Cell length (L_{Mr}) (µm)	Cell width (W_{Mr}) (µm)	Jump duration (t_{jump}) (ms)	Maximum jump speed (U_{max}) (mm s^{-1})	(L_{Mr} s^{-1})	Jump distance (d_{jump}) (µm)	(L_{Mr})
Mean ± SD	23.7 ± 2.4	18.1 ± 2.5	51 ± 9	5.9 ± 1.4	251.4 ± 53.7	97 ± 32	4.2 ± 1.4
Range	19.8–29.0	14.2–22.5	40–85	1.9–8.7	88.6–379.6	41–205	2.0–9.4
n	34	34	36	36	35	36	35

B. Sinking

	Cell length (L_{Mr}) (µm)	Cell width (W_{Mr}) (µm)	Averaged sinking speed (U_{sink}) (µm s^{-1})	(L_{Mr} s^{-1})
Mean ± SD	24.0 ± 2.8	18.9 ± 3.1	66 ± 22	2.7 ± 0.8
Range	17.9–26.2	12.9–23.2	37–108	1.6–4.1
n	8	8	8	8

C. Spontaneous jumping while towing a captured cryptophyte *Teleaulax amphioxeia*

	M. rubrum		*T. amphioxeia*		Jump duration	Maximum jump speed (U_{max})		Jump distance (d_{jump})	
	Cell length (L_{Mr}) (µm)	Cell width (W_{Mr}) (µm)	Cell length (L_{Ta}) (µm)	Cell width (W_{Ta}) (µm)	(t_{jump}) (ms)	(mm s^{-1})	(L_{Mr} s^{-1})	(µm)	(L_{Mr})
Mean ± SD	25.2 ± 3.2	21.2 ± 3.5	13.4 ± 2.1	7.1 ± 1.0	42 ± 5	4.9 ± 1.3	199.4 ± 43.4	79 ± 28	3.2 ± 0.9
Range	21.6–30.4	16.4–26.9	10.9–17.1	5.1–8.1	34–49	3.0–7.0	128.2–276.7	33–126	1.4–4.4
n	7	7	7	7	10	10	10	10	10

D. Sinking while towing a captured cryptophyte *T. amphioxeia*

	M. rubrum		*T. amphioxeia*		Averaged sinking speed (U_{sink})	
	Cell length (L_{Mr}) (µm)	Cell width (W_{Mr}) (µm)	Cell length (L_{Ta}) (µm)	Cell width (W_{Ta}) (µm)	(µm s^{-1})	(L_{Mr} s^{-1})
Mean ± SD	23.0 ± 2.0	18.7 ± 2.0	12.4 ± 0.4	7.4 ± 0.6	95 ± 31	4.2 ± 1.5
Range	21.6–25.3	16.4–20.0	12.0–12.8	6.8–8.0	71–130	3.3–5.9
n	3	3	3	3	3	3

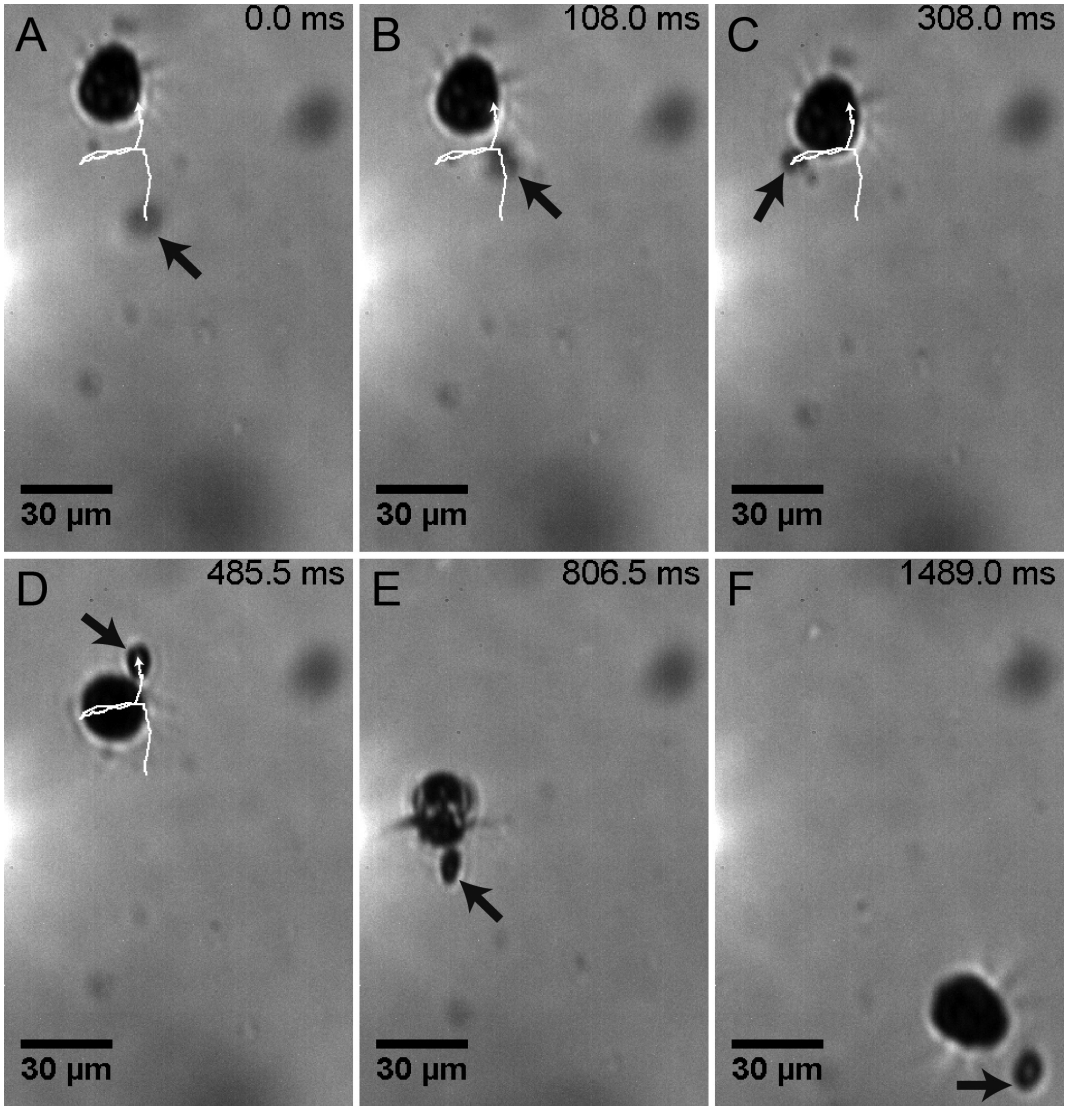

Fig. 4. Time course image sequence illustrating a successful capture of a *Teleaulax amphioxeia* cell by a *Mesodinium rubrum* cell (Event A of Video Group S2). From 0 to 485.5 ms, the *T. amphioxeia* cell swam around the *M. rubrum* cell (A–D). At ~459.5 ms, the cryptophyte was near the ciliate's oral tentacles, and the ciliate started to pull back and be ready for an attack. At ~485.5 ms, the ciliate predator attacked the cryptophyte prey with a poking movement aimed at the ventral posterior part of the prey cell (D). Subsequently, the predator poked the prey 16 times in ~1 s (D–F). The white arrowed lines in (A–D) show the trajectory of the prey before the predator attacked the prey, while the large black arrow in each panel points to the prey

the predator's oral tentacles (Fig. 4D). The prey responded by jumping to the other side of the predator, while the predator also turned quickly towards the fleeing prey and poked the prey 16 times in ~1 s (Fig. 4D,F). In contrast, in an unsuccessful ambush-feeding event (Event B of Video Group 2), when a *T. amphioxeia* prey was swimming with its anterior directly facing an *M. rubrum* predator (Fig. 5C,D), the predator responded quickly by pulling back and using its oral tentacles to poke the anterior of the prey twice (Fig. 5D), but the prey was still able to turn and quickly swim away while the predator failed to pursue with additional poking movements (Fig. 5E,F). All 7 observed successful capture events involved multiple poking movements on the prey by the predator, while in all 3 observed unsuccessful events, the prey was only poked once or twice at its anterior. The poking movements by *M. rubrum* were of high speeds (4.7 ± 1.2 mm s^{-1}), high accelerations (1.9 ± 0.3 m s^{-2}), short durations (37 ± 11 ms), and high numbers of pokes per second (11.7 ± 3.3) (Table 5C).

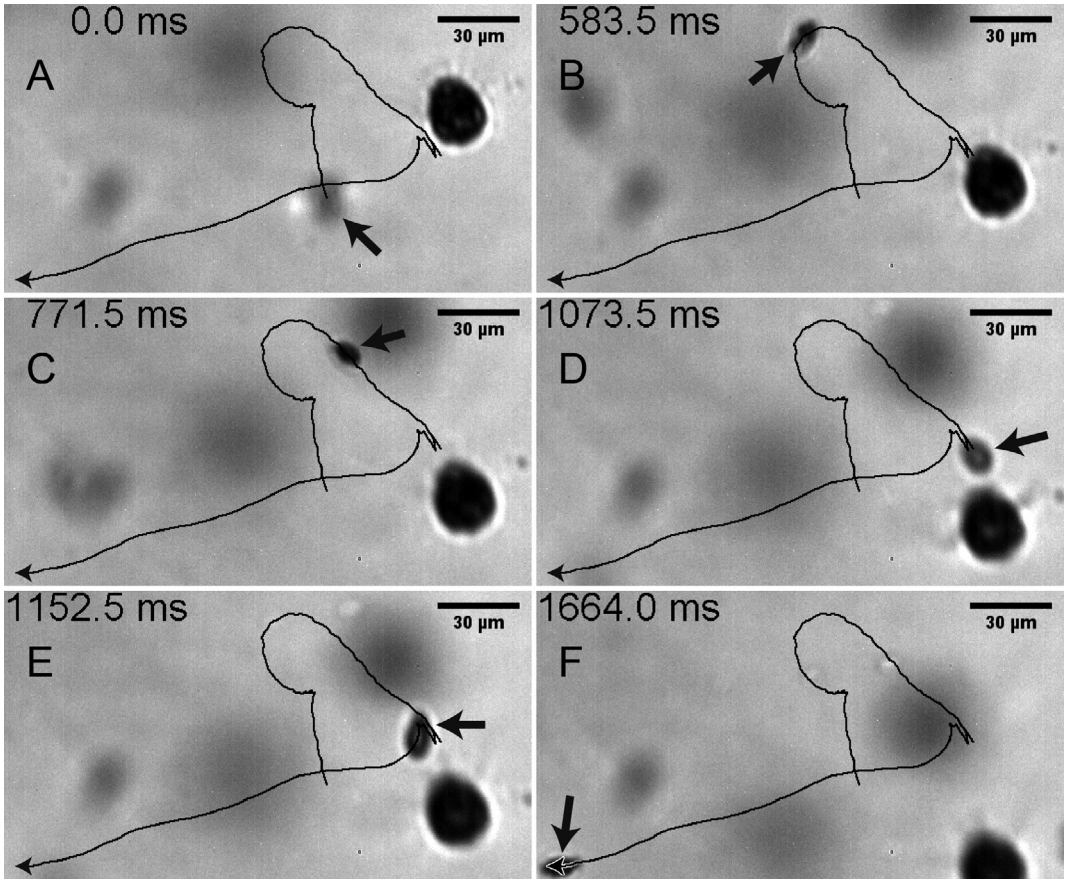

Fig. 5. Time course image sequence illustrating an unsuccessful capture attempt by a *Mesodinium rubrum* cell towards a *Teleaulax amphioxeia* cell (Event B of Video Group S2). From 0 to 1073.5 ms, the *T. amphioxeia* cell swam closer to the *M. rubrum* cell (A–D). At ~1046.5 ms, the cryptophyte swam anterior first towards the ciliate's oral tentacles, and the ciliate started to pull back and be ready for an attack. At ~1073.5 ms, the predator poked twice the anterior part of the prey cell (D), but the prey was still able to turn (E) and quickly swim away (F). In each panel, the black arrowed line shows the trajectory of the prey, while the large black arrow points to the prey

The cryptophyte *T. amphioxeia* sometimes responded remotely to a nearby sinking or moving *M. rubrum* in 2 different ways. First, when a *T. amphioxeia* cell swam slowly towards a motionlessly sinking *M. rubrum* cell, the former remotely detected the latter and subsequently turned and quickly swam away (Fig. 6A; Event A of Video Group S3 at www.int-res.com/articles/suppl/a086p169_supp/). Swimming speeds of *T. amphioxeia* right before avoiding *M. rubrum* were 48 ± 23 µm s^{-1} (Table 5B), significantly slower than those of the *T. amphioxeia* cells that were responded to first by the *M. rubrum* cells (189 ± 70 µm s^{-1} [Table 5A]; Student's *t*-test, p = 0.02; Fig. 7A). Also, reaction distances of *T. amphioxeia* reacting to *M. rubrum* were larger than those of *M. rubrum* reacting to *T. amphioxeia*, albeit not statistically significant (18 ± 10 µm [Table 5B] vs. 8.2 ± 8.2 µm [Table 5A]; Fig. 7B).

Second, an initially motionless *T. amphioxeia* cell was near an *M. rubrum* predator that had just tried unsuccessfully to capture another *T. amphioxeia* cell. Likely, the nearby untargeted *T. amphioxeia* cell was alerted by the flow disturbance imposed by the attacking predator and responded by starting to tumble (Fig. 6B; Event B of Video Group S3). A *T. amphioxeia* prey that had just evaded an *M. rubrum* predator's attack could also start to tumble, as occasionally observed. Such tumbling motions of *T. amphioxeia* prey as responses to nearby *M. rubrum* predators were similar to those of the cryptophyte *S. major* in normal swimming but faster, i.e. shorter in tumble period (Fig. 8; 782 ± 126 vs. 515 ± 269 ms; Student's *t*-test, p = 0.059).

The ciliate *M. rubrum* sometimes jumped away from a fast-approaching *T. amphioxeia* cell whose anterior faced directly towards the ciliate (Fig. 9A;

Table 5. Analysis summary of the predator–prey interaction between the ciliate *Mesodinium rubrum* (Mr) and the cryptophyte *Teleaulax amphioxeia* (Ta)

A. *M. rubrum* reacting to *T. amphioxeia*

	M. rubrum		*T. amphioxeia*		Event duration (ms)	Reaction distance (R_{Mr}) (µm)	*T. amphioxeia* speed when *M. rubrum reacting* (U_{Ta}) (µm s^{-1})
	Cell length (L_{Mr}) (µm)	Cell width (W_{Mr}) (µm)	Cell length (L_{Ta}) (µm)	Cell width (W_{Ta}) (µm)			
Mean ± SD	25.6 ± 4.3	20.0 ± 3.2	13.7 ± 1.8	6.1 ± 1.1	1307.6 ± 664.1	8.2 ± 8.2	189 ± 70
Range	20.3–34.1	17.4–26.5	12.0–16.5	5.2–8.3	187.5–2013.5	0–19	89–254
n	7*	7	7	7	7	6	4

*Consisting of 4 events in which *M. rubrum* attacked *T. amphioxeia* and 3 events in which *M. rubrum* evaded *T. amphioxeia*

B. *T. amphioxeia* avoiding *M. rubrum*

	M. rubrum		*T. amphioxeia*		Event duration (ms)	Reaction distance (R_{Ta}) (µm)	*T. amphioxeia* speed before avoiding *M. rubrum* (U_{Ta}) (µm s^{-1})
	Cell length (L_{Mr}) (µm)	Cell width (W_{Mr}) (µm)	Cell length (L_{Ta}) (µm)	Cell width (W_{Ta}) (µm)			
Mean ± SD	20.9 ± 3.2	16.6 ± 3.4	13.3 ± 1.3	6.3 ± 1.3	1459.5 ± 363.1	18 ± 10	48 ± 23
Range	17.9–24.2	12.9–19.6	12.0–14.5	5.4–7.8	1100.5–1826.5	9–29	21–64
n	3	3	3	3	3	3	3

C. Kinematics of the poking movements done by *M. rubrum* to capture a *T. amphioxeia*

	M. rubrum		*T. amphioxeia*		Average time of a poke (t_{poke}) (ms)	Path-averaged speed (U_{ave}) (µm s^{-1}) (L_{Mr} s^{-1})	Maximum speed (U_{max}) (mm s^{-1}) (L_{Mr} s^{-1})	Maximum acceleration (a_{max}) (m s^{-2}) (× 10^4 L_{Mr} s^{-2})	NGDR	Number of pokes s^{-1}
	Cell length (L_{Mr}) (µm)	Cell width (W_{Mr})(µm)	Cell length (L_{Ta}) (µm)	Cell width (W_{Ta}) (µm)						
Mean ± SD	23.9 ± 2.2	19.4 ±1.5	13.7 ± 1.8	7.1 ± 1.1	37 ± 11	472 ± 94	198.2 ± 60.8	1.9 ± 0.3	8.0 ± 1.7	0.274 ± 0.207	11.7 ± 3.3
Range	21.0–27.2	17.4–21.1	12.1–17.1	5.4–8.4	25–60	379–616	126.6–309.2	1.5–2.3	6.0–10.1	0.099–0.556	7.9–17.0
n	7	7	7	6	7	5	7	7	7	6	6

Event A of Video Group S4 at www.int-res.com/articles/suppl/a086p169_supp/) or from a *T. amphioxeia* cell that bumped quickly into the ciliate's oral tentacles with its anterior (Fig. 9B; Event B of Video Group S4).

After successfully capturing a *T. amphioxeia* prey, an *M. rubrum* predator performed spontaneous jumps while towing the captured prey (Event A of Video Group S5 at www.int-res.com/articles/suppl/a086p169_supp/) before ingesting the prey. In a rather peculiar event that was observed (Event B of Video Group S5), an *M. rubrum* predator captured a *T. amphioxeia* prey but eventually released it and jumped away. Probably, the prey was too big to ingest. Amazingly, the *T. amphioxeia* prey appeared intact and was still able to swim and jump to avoid another *M. rubrum* cell.

4. DISCUSSION

4.1. Prey encounter, detection, and capture by *Mesodinium rubrum*

The ciliate *M. rubrum* is an active ambush predator that passively encounters and detects, via mechanoreception, a swimming prey and then actively attacks it for capture. Thus, the swimming behavior of its cryptophyte prey plays an important role in determining *M. rubrum*'s prey encounter rate as well as prey detection and identification via hydrodynamic signal perception.

First, the encounter rate between *M. rubrum* and its cryptophyte prey depends on the swimming speed of the prey. The encounter kernel between *M. rubrum* and its prey *Teleaulax amphioxeia*, i.e. the maximum clearance rate, can be calculated as $\pi\ (a + R_{Mr})^2\ U_{ave}$, where a (= 10.9 µm) is the mean equivalent spherical radius of *M. rubrum*, R_{Mr} (= 8.2 µm) is the mean reaction distance of *M. rubrum* to *T. amphioxeia* (measured as the nearest surface-to-surface distance), and U_{ave} (= 155 µm s^{-1}) is the mean path-averaged speed of *T. amphioxeia*. The calculated maximum clearance rate is 0.015 ml d^{-1}, ~33 *M. rubrum* body volumes per day in terms of the specific clearance rate. This value is 4 to 5 orders of magnitude lower than the necessary specific clearance rate required to maintain a population (i.e. on the order of 10^6 body volumes per day; Kiørboe 2011; see also Fig. 3.1 in Fenchel 1987). This low value is, however, consistent with the

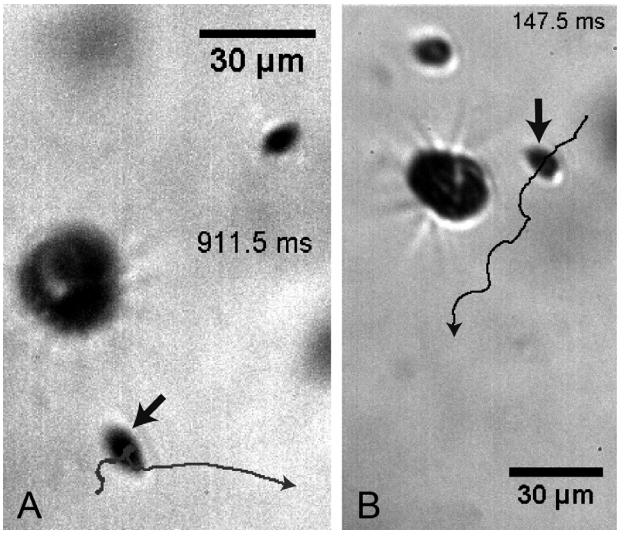

Fig. 6. Image frames extracted from videos illustrating the behavioral reactions of the cryptophyte *Teleaulax amphioxeia* to the ciliate *Mesodinium rubrum*. (A) While swimming upward, a *T. amphioxeia* cell remotely detected the head-on approach of a sinking ciliate *M. rubrum* and immediately turned and quickly swam away (Event A of Video Group S3). (B) An initially motionless *T. amphioxeia* cell was near a ciliate *M. rubrum* that had just tried unsuccessfully to capture another *T. amphioxeia* cell. Immediately, the former *T. amphioxeia* cell started to tumble (Event B of Video Group S3). In each panel, the black arrowed line shows the trajectory of the cryptophyte, while the large black arrow points to the cryptophyte

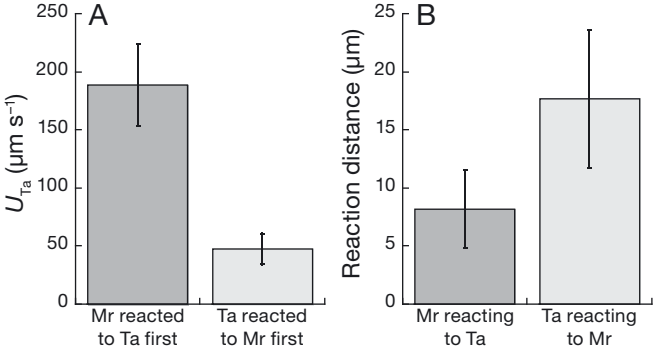

Fig. 7. Observed events where a *Teleaulax amphioxeia* (Ta) cell swam towards a motionlessly sinking *Mesodinium rubrum* (Mr) cell. (A) The mean of the Ta swimming speeds (U_{Ta}, µm s^{-1}) of those events where Ta reacted to Mr first was significantly smaller than that where Mr reacted to Ta first and (B) the mean of the reaction distances of Ta reacting to Mr was larger than that of Mr reacting to Ta but not statistically significant, with large variances. Error bars represent SEs

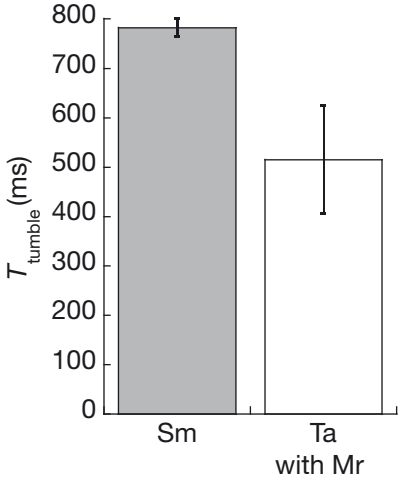

Fig. 8. Comparison of cryptophyte tumble period (T_{tumble}, ms) for 2 different species and situations, i.e. *Storeatula major* in normal swimming (Sm) and *Teleaulax amphioxeia* in responding to a nearby ciliate predator *Mesodinium rubrum* (Ta with Mr). Error bars represent SEs

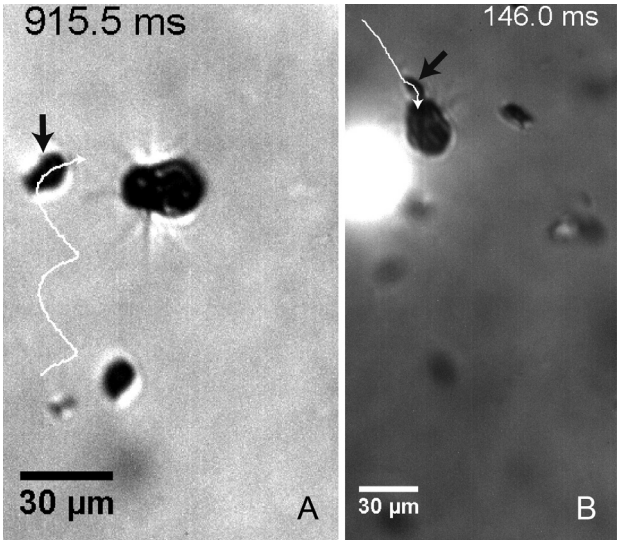

Fig. 9. Image frames extracted from videos illustrating the jumping-away reactions of the ciliate *Mesodinium rubrum* to the cryptophyte *Teleaulax amphioxeia*. (A) A ciliate *M. rubrum* jumped away from a *T. amphioxeia* cell that was swimming towards the ciliate with its anterior facing the ciliate (Event A of Video Group S4). (B) A ciliate *M. rubrum* jumped away from a *T. amphioxeia* cell that was swimming and bumping into the ciliate's oral tentacles with its anterior (Event B of Video Group S4). In each panel, the white arrowed line shows the trajectory of the cryptophyte, while the large black arrow points to the cryptophyte

fact that *M. rubrum* is almost entirely phototrophic (Johnson & Stoecker 2005). Nevertheless, the calculated maximum clearance rate results in an encounter rate of ~22 *T. amphioxeia* cells per day, if a mean *T. amphioxeia* concentration of 1432 cells ml^{-1} is assumed (based on the data reported by Johnson et al. [2013]). By further assuming a capture success rate of 5%, this encounter rate leads to ~1 cell d^{-1} ingestion

rate, thereby being sufficient for temperate *M. rubrum* to achieve its maximum growth rate (Smith & Hansen 2007). In contrast, for *Storeatula major* and *Guillardia theta*, R_{Mr} ~ 0 and U_{ave} = 64 and 57 µm s^{-1}, respectively; also, the field concentrations of *S. major* and *G. theta* are usually much lower than that of *T. amphioxeia*. Thus, these 2 cryptophyte species cannot supply sufficient encounter rates for *M. rubrum* to achieve its maximum growth rate.

Second, a swimming prey-imposed flow provides the hydrodynamic signal that *M. rubrum* detects; this hydrodynamic signal depends on the swimming speed of the prey. By modeling the flow imposed by a swimming *T. amphioxeia* cell as a stresslet, a threshold flow velocity at the mean reaction distance of *M. rubrum* to *T. amphioxeia* can be estimated as $U_{ave}\ a_{Ta}{}^2 / (a_{Ta} + R_{Mr})^2$, where a_{Ta} (= 4.6 µm) is the mean equivalent spherical radius of *T. amphioxeia*. The calculated threshold flow velocity of ~20 µm s^{-1} falls in the range of 15 to 42 µm s^{-1} determined previously for the heterotrophic ciliate *M. pulex* by Jakobsen et al. (2006), suggesting that these *Mesodinium* species may share a similar range of threshold flow velocity for prey detection. On the other hand, the swimming speeds of the cryptophytes *S. major* and *G. theta* are only small fractions of that of *T. amphioxeia*. Thus, their imposed flows are much weaker, mostly below the calculated threshold flow velocity except for the region within ~3 µm from their cell surface. Within such a close range, *M. rubrum* has difficulty maneuvering quickly and precisely to attack and capture the prey (e.g. pulling back for an attack). These estimations are consistent with the previously mentioned observations in which *M. rubrum* were offered the slow-moving *S. major* or *G. theta* but did not attempt an attack and the fact that neither *S. major* (Peltomaa & Johnson 2017) nor *G. theta* (Hansen et al. 2012) supports the growth of *M. rubrum*.

Finally, with regard to prey attack and capture, the HSMIS observations suggest that it is probably necessary for *M. rubrum* to use oral tentacles to initially poke a detected *T. amphioxeia* prey's ventral posterior part to make the prey lose its escape ability. Otherwise, if the prey's anterior is poked initially, the prey is still able to escape. The forked apical ends of *Mesodinium* tentacles are known to possess extrusomes, which are suspected to be involved in prey capture; however, their specific purpose remains undocumented (Lindholm et al. 1988, Moestrup et al. 2012, Nam et al. 2012). Previous studies have noted that prey become immobilized following contact with the oral tentacles of *M. rubrum* (Yih et al. 2004), *M.* cf. *chamaeleon* (Hargraves 1991), and *M. pulex* (Jakobsen et al. 2006). The present observations clearly illustrate that *M. rubrum* uses its tentacles to immobilize *Teleaulax* prey by repeated fast jabs, which presumably result in the discharging of extrusomes into the prey. While the present study observed that successful attacks with tentacles by *M. rubrum* only involved contacting the ventral posterior part of *Teleaulax* prey, the significance of this observation remains unclear. Possibly the ciliate was afforded more time since it was chasing its prey from the posterior, thereby allowing more opportunities to poke its prey with extrusomes, or perhaps this part of the cell has a weaker pellicle compared with the anterior.

From the point of view of the predator, it may be necessary for *M. rubrum* to perceive the instantaneous velocity and trajectory of the *T. amphioxeia* prey to increase the chance to poke the prey's ventral posterior part when initiating an attack. It is feasible for *M. rubrum* to do so by monitoring the spatiotemporal pattern of the flow field imposed by the nearby swimming prey, similar to what has been shown previously for the copepod *Oithona plumifera* ambush feeding on ciliate prey (Jiang & Paffenhöfer 2008). This notion receives support from the following HSMIS observations: (1) The reaction distances of *M. rubrum* to *T. amphioxeia* had a wide variance (8.2 ± 8.2 µm [mean ± SD]); (2) *M. rubrum* waited to attack the prey at a seemingly optimal position; and (3) *M. rubrum* did not initiate an attack but jumped away when a prey's anterior was bumping into the predator's oral tentacles. In contrast, *M. rubrum* was not observed to even attempt an attack on the cryptophytes *S. major* and *G. theta*, probably because their slow swimming speeds and looped or curved trajectories make it impossible for *M. rubrum* to perceive their instantaneous velocity and trajectory.

Although similar in the mechanisms of prey encounter and detection, the heterotrophic *M. pulex* achieves an ingestion rate of ~25 prey cells d^{-1} (Tarangkoon & Hansen 2011), much higher than that achieved by the mixotrophic but dominantly phototrophic *M. rubrum*. The ingestion rate of *M. pulex* more or less supports 1 cell division per day (i.e. *M. pulex* cell volume = 1471 µm^3, *Teleaulax* sp. cell volume = 105 µm^3, and gross growth efficiency ~56%; Tarangkoon & Hansen 2011). These differences could be driven by differences in capture efficiency or innate ingestion requirements. For instance, *M. pulex* could have more powerful oral tentacles that may immobilize prey more easily; however, it is unclear if it only needs to poke its prey once to immobilize it, due to the low frame rate of 30 frames s^{-1}

used in the previous observations by Jakobsen et al. (2006). Also, limitation of the prey ingestion rate by *M. rubrum* is due to lower requirements for ingesting prey, based on their retention rather than digestion of prey contents and their reliance on prey photosynthetic metabolism (Lasek-Nesselquist et al. 2015); however, despite only requiring 1 prey d^{-1} to maintain a maximum growth rate (Smith & Hansen 2007), *M. rubrum* are capable of luxury uptake of prey (>10 ingested per day) that is likely an adaptation to exploit abundant prey (given the opportunity) to sustain growth (Peltomaa & Johnson 2017).

4.2. Predator detection and avoidance by cryptophyte prey

The HSMIS observations show that in one situation, where a cryptophyte *T. amphioxeia* cell swam slowly (48 ± 23 µm s^{-1}) towards a motionlessly sinking *M. rubrum* cell, the former remotely detected the latter and reacted first by escaping. In contrast, in another situation, where a *T. amphioxeia* cell swam fast (189 ± 70 µm s^{-1}), the *M. rubrum* predator reacted to the *T. amphioxeia* prey first. Also, the reaction distance of the prey (18 ± 10 µm) was farther than that of the predator (8.2 ± 8.2 µm). Thus, in the first situation, right before reacting to the *M. rubrum* predator, the slow-swimming *T. amphioxeia* cell imposed a flow that was weaker and farther from the predator compared with the flow imposed by the fast-swimming *T. amphioxeia* cell in the second situation, where the predator reacted to the prey first. As a result, the *M. rubrum* predator was unlikely to detect the *T. amphioxeia* prey via mechanoreception in the first situation.

Nevertheless, the *T. amphioxeia* prey experienced a hydrodynamic interaction with the *M. rubrum* predator once the former approached the latter close enough. Consequently, a flow disturbance was generated around the *T. amphioxeia* cell, which provided the hydrodynamic signal for the slow-swimming *T. amphioxeia* cell to detect the predator. A question, however, may be asked: Why didn't the fast-swimming *T. amphioxeia* cell detect the *M. rubrum* predator in the same way? The fast-swimming *T. amphioxeia* cell imposed, around itself, a much stronger flow that probably masked the flow distance generated by the hydrodynamic interaction, thereby preventing the fast-swimming *T. amphioxeia* cell from detecting the predator. While this study has no evidence of chemoreception playing an important role in the detection of prey or predator, it is possible that such sensing mechanisms also play some role. Particularly, once *M. rubrum* has captured *Teleaulax* prey, it may recognize some cell surface characteristic that signals ingestion to proceed. It is also possible that changes in slow-swimming *Teleaulax* prey behavior in response to motionlessly sinking *Mesodinium* may be due to detection of a chemical gradient released from its predator (Event A of Video Group S3). Hydrodynamic interactions between protistan swimmers can be an important mechanism for generating the hydrodynamic signals that mediate protistan predator–prey interactions. Further investigations are needed to shed light on this topic by using theoretical hydrodynamic models and computational fluid dynamics simulations. The concept of hydrodynamic interaction has been previously proposed to understand the generation of hydrodynamic signals between 2 similar-sized copepods (Jiang et al. 2002) and between a copepod predator and its copepod nauplius prey (Jiang & Paffenhöfer 2004). The rate of deformation was previously proposed as the hydrodynamic signal that 2 small flagellates, *Chrysochromulina simplex* and *Gymnodinium flagellare*, perceived when exposed to predator-generated feeding currents (9–12 s^{-1}; Jakobsen 2002). In the present study, however, the *T. amphioxeia* prey was not that small compared with the *M. rubrum* predator (4.6 vs. 10.9 µm in terms of the mean equivalent spherical radius), and the *M. rubrum* predator did not generate a feeding current at all but only sank slowly while the *T. amphioxeia* prey swam nearby along its own trajectory. Thus, it is impossible to calculate the rate of deformation as in the case of predator-generated feeding currents, while the above-described hydrodynamic interaction offers a more reasonable explanation in eliciting such a response.

With regard to predator avoidance, the tumbling motions observed for some *T. amphioxeia* cells following contact with *M. rubrum* as well as for *S. major* in general may be an effective anti-predator defense behavior that prevents *M. rubrum* from accurately poking the ventral posterior part of the cryptophyte prey.

The above-discussed behavioral characteristics of the *Mesodinium*–cryptophyte predator–prey interaction support the notion that predator–prey interactions in marine planktonic protists are evolutionary arms races. A similar support is provided by the predator–prey interaction between the dinoflagellate *Dinophysis acuminata* and the ciliate *M. rubrum*: the predator has developed a suite of behaviors to encounter, detect, attack, and capture the prey efficiently and effectively, while the prey is also skillful at detecting and avoiding the predator (Jiang et al. 2018).

4.3. Trade-offs of different swimming behaviors in cryptophytes

The photosynthetic cryptophyte algae are ubiquitous in marine, coastal, and freshwater ecosystems (Klaveness 1988, Hoef-Emden & Archibald 2017, Johnson et al. 2018). With their unique green light-harvesting phycobiliproteins, cryptophytes are capable of photosynthesis in low-light environments (Spear-Bernstein & Miller 1989, Doust et al. 2006). They can be highly abundant; for example, cryptophytes, after diatoms and dinoflagellates, contributed more than 5% to cumulative phytoplankton biomass in San Francisco Bay (Cloern & Dufford 2005), and cryptophyte mean concentration of 1432 cells ml^{-1} with a span of 15720 cells ml^{-1} was observed over multiple years in Chesapeake Bay (Johnson et al. 2013).

Cryptophytes likely face high predation pressure in the field (Johnson et al. 2018). They are known to be nutrient-rich prey, with 1 study demonstrating that they possessed the highest per volume content of carbon, nitrogen, chl *a*, starch, carbohydrates, and protein among an array of phytoplankton (Moal et al. 1987). Besides being essential prey for *M. rubrum*, cryptophytes are preyed upon by other ciliates (Stoecker & Silver 1990, Jakobsen & Hansen 1997) and phagotrophic dinoflagellates (Larsen 1988, Skovgaard 1998, Jeong et al. 2005, Johnson 2015) and are fed upon selectively by copepods (Meyer-Harms & von Bodungen 1997, Cotonnec et al. 2001, Khanaychenko et al. 2018).

Different swimming behaviors of cryptophyte algae may present trade-offs between resource acquisition and predation risk. Compared with the slow-swimming *S. major* and *G. theta*, *T. amphioxeia* cells swim much faster, thereby competing better for light and nutrients but also facing much higher predation risk from their specialized predator, *M. rubrum*. A fast-swimming cell imposes a strong flow that can be easily detected by the ambush-feeding predator; also, the strong flow probably masks the predator-induced flow disturbance, causing difficulty in detecting the predator. In contrast, a slow-swimming cell imposes a weak flow that mostly is below the detection threshold of the predator; also, the flow is too weak to interfere with detecting the predator-induced flow disturbance. Thus, slow swimming is effective not only in reducing the prey-imposed hydrodynamic signal but also in increasing the sensitivity to detect the predator via mechanoreception. Slow swimming is, however, not ideal for competing for light and nutrients. *Teleaulax* spp. are often the most abundant (Massana et al. 2004, Johnson et al. 2016) and fastest-growing (Johnson et al. 2018) cryptophytes in coastal ecosystems and may therefore be selectively grazed by ciliates and dinoflagellates. The fact that *Teleaulax* spp. are preferred prey of *M. rubrum* may be at least partially explained by their relatively high availability and detectability via hydrodynamic signal perception as well as the ambush-feeding mechanism of the ciliate.

Above all, the individual-level behavioral characteristics of swimming, predator–prey encounter and perception, prey attack and capture, and predator defense and avoidance strongly delimit the trophic link from cryptophytes to the ciliate *M. rubrum*. While the present results underscore the important role of predator–prey dynamics in driving prey selection, in the case of *M. rubrum*, this has also driven adaptations for compatibility of which cryptophyte species the ciliate can exploit for organelles. Clearly, specialization in prey and organelle selection in *M. rubrum* has driven adaptation within this species complex towards increasing reliance on acquired metabolism (Johnson & Stoecker 2005, Lasek-Nesselquist et al. 2015). The present results have provided a mechanistic understanding for the role of trophic dynamics and behavior in shaping niche space and cellular and metabolic innovation in *M. rubrum*. In doing so, they also support a fundamental role for these processes in shaping the evolution of acquired phototrophy and symbiogenesis in eukaryotes.

The present study suggests that the swimming behavior of cryptophyte prey species affects prey preference of *M. rubrum*. With regard to prey selection in protistan predator–prey interactions, other critical factors that affect prey selection include prey size and shape, prey chemical composition and nutritional quality, and the presence of certain infochemicals (e.g. Hansen & Calado 1999, Wolfe 2000, Tillmann 2004, Harvey et al. 2013).

It is also worth noting that the behaviors and motility patterns that the present study has observed for cryptophytes are likely widespread across multiple flagellate groups. For example, the haptophyte *C. simplex* and the dinoflagellate *G. flagellare* were observed to display escape responses to predator-generated feeding currents (Jakobsen 2002). The dinoflagellates *Heterocapsa rotundata* and *G. simplex* along with the cryptophyte *Rhodomonas salina* were found to display different motility patterns, including slow and fast swimming and escape responses, when facing the ambush predator *M. pulex* (Jakobsen et al. 2006). It is of fundamental importance to investigate the individual-level behaviors and species interactions, as well as the morphologi-

cal, physiological, and hydrodynamic traits and trade-offs of flagellates to gain a mechanistic understanding of the roles that flagellates play at the base of the marine food web.

Acknowledgements. H.J. was supported by National Science Foundation (NSF) grants OCE-1433979 and OCE-1559062. M.D.J. was supported by NSF grant IOS-1354773. Both M.D.J. and H.J. gratefully acknowledge a Woods Hole Oceanographic Institution 2015 Interdisciplinary Study Award to them. The authors thank Hans Jakobsen and 2 anonymous reviewers for providing helpful and constructive comments that improved the manuscript.

LITERATURE CITED

Altenburger A, Blossom HE, Garcia-Cuetos L, Jakobsen HH and others(2020) Dimorphism in cryptophytes — the case of *Teleaulax amphioxeia/Plagioselmis prolonga* and its ecological implications. Sci Adv 6:eabb1611

Buskey EJ (1997) Behavioral components of feeding selectivity of the heterotrophic dinoflagellate *Protoperidinium pellucidum*. Mar Ecol Prog Ser 153:77–89

Cloern JE, Dufford R (2005) Phytoplankton community ecology: principles applied in San Francisco Bay. Mar Ecol Prog Ser 285:11–28

Cotonnec G, Brunet C, Sautour B, Thoumelin G (2001) Nutritive value and selection of food particles by copepods during a spring bloom of *Phaeocystis* sp. in the English Channel, as determined by pigment and fatty acid analyses. J Plankton Res 23:693–703

Doust AB, Wilk KE, Curmi PMG, Scholes GD (2006) The photophysics of cryptophyte light-harvesting. J Photochem Photobiol A 184:1–17

Fenchel T (1987) Ecology of protozoa: the biology of free-living phagotrophic protists. Science Tech Publishers, Madison, WI

Ferrari MCO, Wisenden BD, Chivers DP (2010) Chemical ecology of predator–prey interactions in aquatic ecosystems: a review and prospectus. Can J Zool 88:698–724

Gustafson DE, Stoecker DK, Johnson MD, Van Heukelem WF, Sneider K (2000) Cryptophyte algae are robbed of their organelles by the marine ciliate *Mesodinium rubrum*. Nature 405:1049–1052

Hansen PJ, Calado AJ (1999) Phagotrophic mechanisms and prey selection in free-living dinoflagellates. J Eukaryot Microbiol 46:382–389

Hansen PJ, Moldrup M, Tarangkoon W, Garcia-Cuetos L, Moestrup Ø (2012) Direct evidence for symbiont sequestration in the marine red tide ciliate *Mesodinium rubrum*. Aquat Microb Ecol 66:63–75

Hargraves P (1991) Narrow river phytoplankton. Maritimes 35:6–8

Harvey EL, Jeong HJ, Menden-Deuer S (2013) Avoidance and attraction: chemical cues influence predator–prey interactions of planktonic protists. Limnol Oceanogr 58: 1176–1184

Herfort L, Peterson TD, McCue LA, Crump BC and others (2011) *Myrionecta rubra* population genetic diversity and its cryptophyte chloroplast specificity in recurrent red tides in the Columbia River estuary. Aquat Microb Ecol 62:85–97

Hibberd DJ, Greenwood AD, Griffiths HB (1971) Observations on the ultrastructure of the flagella and periplast in the Cryptophyceae. Br Phycol J 6:61–72

Hoef-Emden K, Archibald JM (2017) Cryptophyta (cryptomonads). In: Archibald JM, Simpson AGB, Slamovits CH (eds) Handbook of the protists, 2nd edn. Springer International, Cham, p 851–891

Jakobsen HH (2002) Escape of protists in predator-generated feeding currents. Aquat Microb Ecol 26:271–281

Jakobsen HH, Hansen PJ (1997) Prey size selection, grazing and growth response of the small heterotrophic dinoflagellate *Gymnodinium* sp. and the ciliate *Balanion comatum* — a comparative study. Mar Ecol Prog Ser 158:75–86

Jakobsen HH, Everett LM, Strom SL (2006) Hydromechanical signaling between the ciliate *Mesodinium pulex* and motile protist prey. Aquat Microb Ecol 44:197–206

Jeong HJ, Yoo YD, Park JY, Song JY and others (2005) Feeding by phototrophic red-tide dinoflagellates: five species newly revealed and six species previously known to be mixotrophic. Aquat Microb Ecol 40:133–150

Jiang H (2011) Why does the jumping ciliate *Mesodinium rubrum* possess equatorially located propulsive ciliary belt? J Plankton Res 33:998–1011

Jiang H, Johnson MD (2017) Jumping and overcoming diffusion limitation of nutrient uptake in the photosynthetic ciliate *Mesodinium rubrum*. Limnol Oceanogr 62:421–436

Jiang H, Paffenhöfer GA (2004) Relation of behavior of copepod juveniles to potential predation by omnivorous copepods: an empirical-modeling study. Mar Ecol Prog Ser 278:225–239

Jiang H, Paffenhöfer GA (2008) Hydrodynamic signal perception by the copepod *Oithona plumifera*. Mar Ecol Prog Ser 373:37–52

Jiang H, Paffenhöfer GA (2020) Vortical feeding currents in nauplii of the calanoid copepod *Eucalanus pileatus*. Mar Ecol Prog Ser 638:51–63

Jiang H, Osborn TR, Meneveau C (2002) Hydrodynamic interaction between two copepods: a numerical study. J Plankton Res 24:235–253

Jiang H, Kulis DM, Brosnahan ML, Anderson DM (2018) Behavioral and mechanistic characteristics of the predator–prey interaction between the dinoflagellate *Dinophysis acuminata* and the ciliate *Mesodinium rubrum*. Harmful Algae 77:43–54

Johnson MD (2015) Inducible mixotrophy in the dinoflagellate *Prorocentrum minimum*. J Eukaryot Microbiol 62: 431–443

Johnson MD, Stoecker DK (2005) Role of feeding in growth and photophysiology of *Myrionecta rubra*. Aquat Microb Ecol 39:303–312

Johnson MD, Oldach D, Delwiche CF, Stoecker DK (2007) Retention of transcriptionally active cryptophyte nuclei by the ciliate *Myrionecta rubra*. Nature 445:426–428

Johnson MD, Stoecker DK, Marshall HG (2013) Seasonal dynamics of *Mesodinium rubrum* in Chesapeake Bay. J Plankton Res 35:877–893

Johnson MD, Beaudoin DJ, Laza-Martinez A, Dyhrman S and others (2016) The genetic diversity of *Mesodinium* and associated cryptophytes. Front Microbiol 7:2017

Johnson MD, Beaudoin DJ, Frada MJ, Brownlee EF, Stoecker DK (2018) High grazing rates on cryptophyte algae in Chesapeake Bay. Front Mar Sci 5:241

Khanaychenko A, Mukhanov V, Aganesova L, Besiktepe S, Gavrilova N (2018) Grazing and feeding selectivity of *Oithona davisae* in the Black Sea: importance of cryptophytes. Turk J Fish Aquat Sci 18:937–949

Kiørboe T (2011) How zooplankton feed: mechanisms, traits and trade-offs. Biol Rev Camb Philos Soc 86:311–339

Kiørboe T, Jiang H, Gonçalves RJ, Nielsen LT, Wadhwa N (2014) Flow disturbances generated by feeding and swimming zooplankton. Proc Natl Acad Sci USA 111: 11738–11743

Klaveness D (1988) Ecology of the Cryptomonadida: a first review. In: Sandgren CD (ed) Growth and reproductive strategies of freshwater phytoplankton. Cambridge University Press, Cambridge, p 105–133

Larsen J (1988) An ultrastructural-study of *Amphidinium poecilochroum* (Dinophyceae), a phagotrophic dinoflagellate feeding on small species of cryptophytes. Phycologia 27:366–377

Lasek-Nesselquist E, Wisecaver JH, Hackett JD, Johnson MD (2015) Insights into transcriptional changes that accompany organelle sequestration from the stolen nucleus of *Mesodinium rubrum.* BMC Genomics 16:805

Lima SL, Dill LM (1990) Behavioral decisions made under the risk of predation: a review and prospectus. Can J Zool 68:619–640

Lindholm T, Lindroos P, Mörk AC (1988) Ultrastructure of the photosynthetic ciliate *Mesodinium rubrum.* Biosystems 21:141–149

Massana R, Balagué V, Guillou L, Pedrós-Alió C (2004) Picoeukaryotic diversity in an oligotrophic coastal site studied by molecular and culturing approaches. FEMS Microbiol Ecol 50:231–243

Meyer-Harms B, von Bodungen B (1997) Taxon-specific ingestion rates of natural phytoplankton by calanoid copepods in an estuarine environment (Pomeranian Bight, Baltic Sea) determined by cell counts and HPLC analyses of marker pigments. Mar Ecol Prog Ser 153:181–190

Moal J, Martin-Jezequel V, Harris RP, Samain JF, Poulet SA (1987) Interspecific and intraspecific variability of the chemical composition of marine phytoplankton. Oceanol Acta 10:339–346

Moestrup Ø, Garcia-Cuetos L, Hansen PJ, Fenchel T (2012) Studies on the genus *Mesodinium* I: ultrastructure and description of *Mesodinium chamaeleon* n. sp., a benthic marine species with green or red chloroplasts. J Eukaryot Microbiol 59:20–39

Myung G, Kim HS, Park JS, Park MG, Yih W (2011) Population growth and plastid type of *Myrionecta rubra* depend on the kinds of available cryptomonad prey. Harmful Algae 10:536–541

Nam SW, Shin W, Coats DW, Park JW, Yih W (2012) Ultrastructure of the oral apparatus of *Mesodinium rubrum* from Korea. J Eukaryot Microbiol 59:625–636

Park JS, Myung G, Kim HS, Cho BC, Yih W (2007) Growth responses of the marine photosynthetic ciliate *Myrionecta rubra* to different cryptomonad strains. Aquat Microb Ecol 48:83–90

Peltomaa E, Johnson MD (2017) *Mesodinium rubrum* exhibits genus-level but not species-level cryptophyte prey selection. Aquat Microb Ecol 78:147–159

Peterson TD, Golda RL, Garcia ML, Li B, Maier MA, Needoba JA, Zuber P (2013) Associations between *Mesodinium rubrum* and cryptophyte algae in the Columbia River estuary. Aquat Microb Ecol 68:117–130

Skovgaard A (1998) Role of chloroplast retention in a marine dinoflagellate. Aquat Microb Ecol 15:293–301

Smith M, Hansen PJ (2007) Interaction between *Mesodinium rubrum* and its prey: importance of prey concentration, irradiance and pH. Mar Ecol Prog Ser 338:61–70

Spear-Bernstein L, Miller KR (1989) Unique location of the phycobiliprotein light-harvesting pigment in the Cryptophyceae. J Phycol 25:412–419

Spero HJ (1985) Chemosensory capabilities in the phagotrophic dinoflagellate *Gymnodinium fungiforme.* J Phycol 21:181–184

Stoecker DK, Silver MW (1990) Replacement and aging of chloroplasts in *Strombidium capitatum* (Ciliophora, Oligotrichida). Mar Biol 107:491–502

Svensen C, Kiørboe T (2000) Remote prey detection in *Oithona similis*: hydromechanical versus chemical cues. J Plankton Res 22:1155–1166

Tarangkoon W, Hansen PJ (2011) Prey selection, ingestion and growth responses of the common marine ciliate *Mesodinium pulex* in the light and in the dark. Aquat Microb Ecol 62:25–38

Tillmann U (2004) Interactions between planktonic microalgae and protozoan grazers. J Eukaryot Microbiol 51: 156–168

Wolfe GV (2000) The chemical defense ecology of marine unicellular plankton: constraints, mechanisms, and impacts. Biol Bull 198:225–244

Yih W, Kim HS, Jeong HJ, Myung G, Kim YG (2004) Ingestion of cryptophyte cells by the marine photosynthetic ciliate *Mesodinium rubrum.* Aquat Microb Ecol 36:165–170

Editorial responsibility: Robert Sanders, Philadelphia, Pennsylvania, USA
Reviewed by: 3 anonymous referees

Submitted: October 24, 2020
Accepted: February 19, 2021
Proofs received from author(s): April 30, 2021